

## CHAPTER 1:

**CORRELATIONS IN CONJUGATED POLYMERS****Z.G. Soos, M.H. Hennessy, and D. Mukhopadhyay***Department of Chemistry, Princeton University, Princeton, NJ 08544, USA*

1. Simple and Subtle Correlations
  - 1.1 Molecules or Bands?
  - 1.2 Excitons, Polarons, and the Band Gap
2. Correlations in Idealized Alternating Chains
  - 2.1 Band to Correlated Crossover
  - 2.2 Vibronic Structure and NLO Spectra
  - 2.3 Stark Profiles of Singlet Excitons
3. Excitons in Conjugated Polymer Films
  - 3.1 Towards Quantitative Fits and Exciton Binding Energies
  - 3.2 Concluding remarks

**1. SIMPLE AND SUBTLE CORRELATIONS**

Simple models are particularly important in describing materials. Hydrogenic orbitals guide our understanding of bonding even as they evolve into accurate molecular orbitals of complex systems. Similarly, particle-in-a-box and Bloch functions underlie general discussions of metals and semiconductors. Molecular and band calculations have achieved impressive quantitative results, well beyond Hückel theory for conjugated molecules or polymers and tight-binding models for metals or semiconductors. The vitality of simple models is nevertheless assured on simpler, qualitative grounds: they combine physical insight and computational ease with generality and flexibility. Hückel and tight-binding theory are quantum cell models that describe complex systems in terms of active orbitals and transfer integrals. They treat delocalization in extended systems without explicit consideration of atomic or molecular cores.

The striking optical properties of organic dyes motivated initial studies of delocalization. More recently, large nonlinear optical (NLO) responses, promising electroluminescence, and photo or dopant-induced conductivity have been the focus of experimental and theoretical studies of conjugated polymers. Their novel electronic and optoelectronic properties are unequivocally associated with delocalized  $\pi$ -electrons, and more precisely with real or virtual  $\pi$ - $\pi^*$  excitations. The direct involvement of *excited states* is the reason for discussing correlation effects that are beyond single-particle theory. We will do so in the context of  $\pi$ -electrons with Coulomb interactions. The Pariser-Parr-Pople model<sup>1,2</sup> for conjugated molecules contains approximations subsequently used by Hubbard<sup>3</sup> for transition metals and by Soos and Klein<sup>4</sup> for ion-radical and charge-transfer organic crystals.

Increasingly accurate single-particle methods are being applied to conjugated molecules and polymers, either for all electrons in *ab initio* calculations or for valence electrons in semiempirical schemes. These orbital representations are particularly useful for determining the geometry and ground-state potential surface. The geometry is an input for simple models of active electrons and excited states. Polymer ionization potentials, electron affinities, and band gaps are also amenable to systematic orbital analysis, as discussed by Brédas<sup>5</sup> and Suhai.<sup>6</sup> While configuration interaction (CI) calculations provide a general treatment of correlations, the large basis sets required for all electrons sharply restrict the analysis. The expected gain in accuracy is not evident in current studies of excitation energies. More significantly, direct comparisons among conjugated polymers with similar backbones are far more transparent in  $\pi$ -electron models.

Single-particle descriptions become substantially more powerful when electron-electron correlation is anticipated. We identify *simple* correlation effects as orbital theory plus low-order perturbation corrections. Simple correlations often account for the splitting and ordering of degenerate states. Orbital descriptions are satisfactory even when quantitative analysis requires elaborate CI. By contrast, *subtle* correlations are qualitative failures of orbital descriptions: the Mott transition or the dissociation of  $H_2$  are subtle correlations due to small overlap. Narrow bands, low dimensionality, and excited states are conducive to subtle correlations; all three appear in conjugated polymers. Correlations are required for the formation of excitons, bound electron-hole pairs. Excitons have been investigated in terms of idealized models<sup>7</sup> that typically have linear electron-phonon coupling. The binding energy depends on the degree of delocalization, which in turn depends on both e-e and e-ph interactions.

Hund's rules summarize Coulomb correlations in atomic ground states. Splittings between the  $^3P$ ,  $^1D$ , and  $^1S$  terms arising from the  $(2p)^2$  configuration of C exceed 1 eV, which is enormous at the resolution of atomic spectra. The fundamental importance of correlations was recognized in the early days of quantum mechanics. The degeneracy of  $(2p)^2$  and confined electrons require going beyond an orbital description. Correlations in the  $(1s)^2$  ground state of He merely raise quantitative issues. Molecules typically have closed electronic shells and nondegenerate ground

states. The lowest excitation, from HOMO to LUMO, gives a degenerate triplet and singlet in single-particle theory. As first noted by Lewis and Kasha, the triplet has lower energy. The proper ordering follows from first-order perturbation theory and, like Hund's rules, illustrates a *simple* correlation. In octahedral complexes of transition metals with 4-8 d-electrons, low and high spin ground states are familiar correlation effects in which orbital filling is modified to incorporate the lower energy of high-spin configurations.

Conjugated polymers illustrate subtle correlations. Exciton formation in extended systems is possible but not forced; the band width and dielectric properties of the system can lead to either outcome. Selection rules for one and two-photon absorption are mutually exclusive in polymers with centrosymmetric backbones; the lowest singlet excitation can be in either manifold.<sup>8</sup> In the finite polyenes investigated by Kohler,<sup>9</sup> the two-photon singlet  $2^1A_g$  is below the intense linear absorption to  $1^1B_u$ . The same order holds in polydiacetylenes (PDAs) and polyacetylene (PA), but  $1^1B_u$  is below  $2^1A_g$  in fluorescent polymers<sup>10</sup> such as polysilanes, polythiophenes, poly(*p*-phenylenevinylene), and substituted PPVs. The 1B/2A order reflects competition between constant correlations in  $2p_z$  orbitals and a variable single-particle energy gap. More generally, subtle correlations appear in other even-parity  $A_g$  states that are poorly represented by a single configuration. The alternancy symmetry<sup>2,11</sup> of conjugated hydrocarbons has a variety of interesting and subtle consequences in excited-state spectra. This symmetry becomes the electron-hole or charge-conjugation symmetry of half-filled Hubbard or Pariser-Parr-Pople models.<sup>12</sup>

In this chapter, we consider manifestations of electronic correlations in conjugated polymers, with special attention to qualitative signatures of subtle effects. We use  $\pi$ -electron models throughout and introduce vibronic or electron-phonon contributions when necessary.<sup>13</sup> Phenomenological descriptions are useful for interpreting NLO spectra and provide a unified, semiquantitative treatment of polymers and molecules. Since models are inherently approximate, the case for excitons, band-to-band transitions, or other conclusions about PDA, PPV and other polymers rests primarily on experiment. To set the stage for specific examples, we introduce two general themes for the electronic structure of conjugated polymers.

### 1.1 Molecules or Bands?

Conjugated polymers are semiconductors, with filled  $\pi$ -bands separated by an energy gap from empty  $\pi^*$ -bands. The lowest triplet and singlet excitations are degenerate in extended systems. Confinement to atoms or molecules leads to a simple correlation that disappears in band theory, where electrons and holes move independently and the relative orientation of their spins is immaterial. Bound electron-hole pairs, or excitons, are possible in general. Triplet, singlet, and charge-transfer excitons occur naturally in organic molecular solids such as anthracene,<sup>14</sup> where small intermolecular overlap yields an oriented gas in zeroth order. The crystal structure of organic solids decisively shows molecular units and accounts for small shifts of electronic or vibrational spectra relative to gas-phase molecules.<sup>15</sup>

Van der Waals contacts, multipolar interactions, or hydrogen bonds indicate weak interchain interactions in conjugated polymers. Delocalization is associated with the backbone that contains thousands of repeat units in high polymers and demands a band approach. The major caveat is that current experiments are performed on films, rather than extended chains, whose conformational degrees of freedom generate short conjugation lengths. Finite segments account for the photophysics and thermochromism of polysilanes<sup>16,17</sup> and similar ideas have been applied to PPV<sup>18</sup> and its derivatives. Segments of 10-20 Si atoms or 5-10 phenyl rings become the "molecular" units forming long flexible strands that comprise the backbone.

We list in Table 1 excitation thresholds for triplets, even and odd-parity singlets, and band-gap excitations in anthracene and PDA-PTS single crystals, and in poly(di-*n*-hexylsilane) and PPV films. The triplet excitation for PDA and PPV are estimates based on polyenes, stilbene and Pariser-Parr-Pople calculations. The other entries are experimental. We have left open the threshold for charge carrying excitations in PPV. This is the band gap, or the band-to-band excitation energy, whose magnitude is discussed in this volume. For reasons summarized in Section 3, the band gap cannot be determined within  $\pi$ -electron theory.

	Triplet, E <sub>T</sub>	Singlet, 1B	Singlet, 2A	Band Gap
Anthracene	1.8	3.1	3.5	4.1
PDA-PTS	~1.1	2.00	1.80	2.5
PDHS	3.4	3.5	4.2	5.2
PPV	~1.6	2.5	2.9	-

Table 1: Energy thresholds, in eV, of anthracene and a polydiacetylene (PDA) crystals, and poly(di-*n*-hexylsilane) and poly(*p*-phenylenevinylene) films.

The different excitation thresholds in Table 1 are evidence for confined, or molecular, excited states rather for free electron-hole pairs in semiconductors. On the other hand, the triplets in Table 1 are not dramatically lower than the singlets and conjugated polymers are diamagnetic. The sharp separation of magnetic and optical excitations in paramagnetic ion-radical organic crystals<sup>4</sup> points to narrower bands, consistent with  $\pi$ - $\pi$  stacking of planar donors or acceptors, and stronger correlation. The thresholds of conjugated polymers resemble those of molecular solids and suggest intermediate correlations<sup>19</sup> found in conjugated molecules.

## 1.2 Excitons, Polarons, and the Band Gap

Singlet excitons are normally associated with linear absorption. The binding energy of 1B in Table 1 is 0.5 eV for PDA crystals and over 1 eV for PDHS films. Accurate binding energies are known for other PDA crystals,<sup>20</sup> both at room and cryogenic temperatures. Even-parity excitons are indicated when 2A has lower energy than 1B, but identification of the binding requires care when the state is poorly represented by an electron-hole pair. Triplet excitons, by contrast, are readily

understood as a bound e-h pair.

A free electron-hole pair defines the band gap, the top line in Fig. 1. In this schematic representation, binding energies of singlet and triplet excitons are measured relative to the band gap. Excitons in silicon or germanium have small binding energies of meV and show hydrogenic spectra that yield the e-h separation. Excitons in  $\text{Cu}_2\text{O}$  also show hydrogenic spectra referenced to the band gap. Such spectra have not been identified in conjugated polymers and would in any case be different for delocalization along a chain. Evidence for excitons then rests on the more difficult, direct determination of both the band gap and binding energy.

The polaron binding energy  $E_r$  is also shown schematically in Figure 1. This stabilization is associated with nuclear relaxation about the cation or anion radical. In the special case of a single polyacetylene (PA) strand, the Su-Schrieffer-Heeger (SSH) model<sup>21,22</sup> accounts in detail for relaxation of charged solitons in infinite Hückel chains with linear e-ph coupling. More generally, both intrachain and interchain relaxation are possible for charges localized on molecules or segments. Accurate evaluation of polaron binding energies is a formidable undertaking. Since PPV fluorescence from 1B coincides

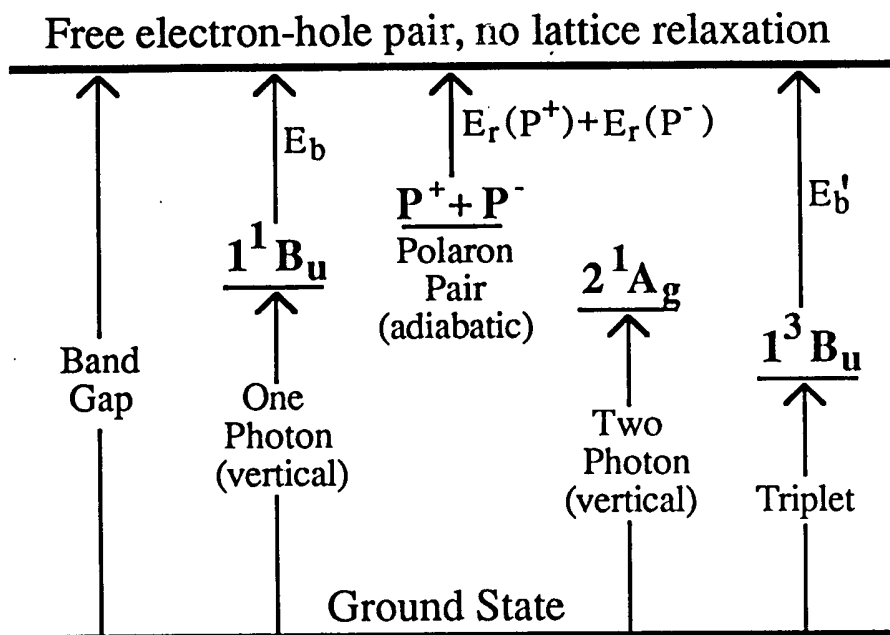


Fig. 1: Schematic energy-level diagram for conjugated polymers. The band gap is the vertical transition to a free electron-hole pair. One and two-photon excitations are vertical from the ground state, while polaron relaxation and exciton binding are relative to the band gap. Relaxation of  $1^1\text{B}_u$  and  $2^1\text{A}_g$  is neglected for simplicity. The adiabatic triplet state has both electronic binding and relaxation from the band gap.

closely with its electroluminescence,<sup>23</sup> singlet excitons are intermediates in the recombination of  $P^+$ ,  $P^-$  injected at the electrodes. Hence  $2E_r$  is less than the singlet-exciton binding energy  $E_b$ ; both  $E_r$  and  $E_b$  are negligible for band-to-band excitation.

## 2. CORRELATIONS IN IDEALIZED ALTERNATING CHAINS

Hückel or tight binding models provide a general approach to excitation energies, NLO responses, and other novel optoelectronic properties of conjugated polymers. Quantum cell models unify, clarify, and quantify observations in chemically diverse systems. The representative polymers shown in Fig. 2 have centrosymmetric backbones in their extended conformation and their unit cells contain an even number of active electrons. They are semiconductors in single-particle theory. The generic polymer, PA, has alternating transfer integrals  $t(1 \pm \delta)$  and band gap  $4t\delta$ . Alternating chains have been crucial for theoretical discussions of e-e and e-ph contributions to conjugated polymers and illustrate the different goals of simple models and direct quantum chemical investigations of specific polymers or oligomers.

The regular ( $\delta = 0$ ) chain is a one-dimensional metal in Hückel theory. Its Peierls instability is modeled in SSH theory<sup>22</sup> by a harmonic  $\sigma$ -framework and linear coupling  $t'(R_0)$  in the Taylor expansion of  $t(R)$ . The analysis of self-localized excitations such as neutral or charged solitons, polarons, or bipolarons continues to motivate solid-state studies and has been extended to polymers with nondegenerate ground states.<sup>21</sup> Although based on Hückel theory and linear e-ph coupling, self-localized states abundantly illustrate subtle, nonlinear, and nonperturbative aspects of excited states in extended systems.

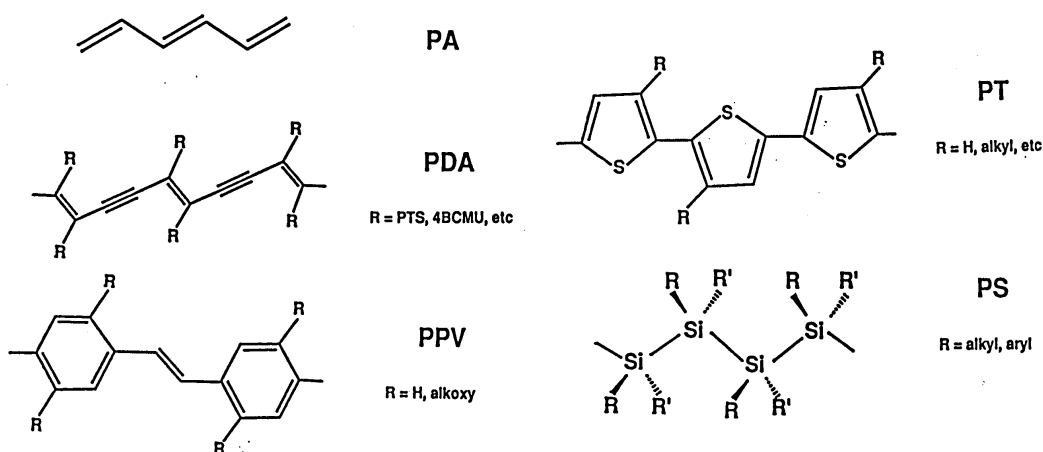


Fig. 2. Centrosymmetric backbones of representative conjugated polymers in their extended conformation.

Lieb and Wu demonstrated<sup>24</sup> the *electronic* instability of regular ( $\delta = 0$ ) chains by solving the Hubbard model for arbitrary on-site repulsion  $U$  and transfer integral  $t$ . Any  $U > 0$  opens a gap in the linear absorption spectrum. Since there is no gap in the two-photon spectrum,<sup>25</sup> *regular* Hubbard chains have  $2^1A_g$  below  $1^1B_u$  for any  $U > 0$ . This correlation result holds for arbitrary spin-independent potentials  $V(R)$  that

conserve electron-hole symmetry.<sup>8</sup> There is no Mott transition in these linear chains: half-filled bands are insulators<sup>24</sup> for  $U > 0$ . The generalization to chains with  $0 \leq \delta \leq 1$  leads to several subtle correlation effects.

## 2.1 Band to Correlated Crossover

Band theory gives a gap  $4t\delta > 0$  for alternating chains, with degenerate  $1^1B_u$ ,  $1^3B_u$  and  $2^1A_g$  at the band edge. Exciton formation may stabilize 1B relative to 2A or the band gap, while 2A becomes a spin wave for  $U \gg t$  and falls below 1B. The relative order of 1B and 2A is a measure of e-e correlation.

The theoretical problem is to follow the evolution of Hückel bands  $\pm \varepsilon(k, \delta)$

$$\varepsilon(k, \delta) / 2t = \sqrt{\cos^2 k + \delta^2 \sin^2 k}, \quad -\pi/2 < k \leq \pi/2 \quad (1)$$

for one electron per site under a potential  $V(R)$ . We have discussed the general case<sup>26,8</sup>

$$V(R) = U \sum_p n_p (n_p - 1) / 2 + \sum_{p < p'} V(p, p') [1 - n_p][1 - n_{p'}] \quad (2)$$

$$V(p, p') = e^2 / \sqrt{\rho^2 + R_{pp'}^2}$$

where  $n_p$  is the number operator. The first term of  $V(R)$  gives the Hubbard chain with  $U = e^2/\rho$ ; the second corresponds to Coulomb interactions among sites separated by  $R_{pp'}$  in Fig. 2. Electron-hole symmetry holds for any  $V(p, p')$ . The Pariser-Parr-Pople model takes  $U = e^2/\rho$  from atomic data. Since  $t(R)$  is also specified in advance, the PPP model<sup>19</sup> for polymers is fixed *a priori* by the geometry. Transferability was a major goal for conjugated molecules<sup>27</sup> and contrasts sharply with solid-state models in which  $t$ ,  $U$  and other parameters are taken from experiment for each system.

The band states (1) evolve as on-site Hubbard  $U$  or long-range  $V(R)$  is turned on. Strong correlation illustrates spin-charge separation: low-energy spin waves are associated with a spin-1/2 chain and antiferromagnetic exchange  $J \sim 2t^2/U$ , while optical excitations around  $U$  involve transfers of electrons localized at each site. Turning on  $V(R)$  is the natural way of thinking about correlations, but difficult to realize physically. The same results hold mathematically for constant  $V(R)$  and variable transfer integrals. The  $2p_z$  orbitals and similar bond lengths of  $\pi$ -conjugated polymers lead to  $t \sim 2.5$  eV and constant  $V(R)$ . The different backbones in Fig. 2 produce a range of band gaps that, in alternating chains, amount to varying  $4t\delta$ . Since  $4t\delta$  sets the scale for correlations in infinite chains, conjugated polymers are rare systems in which variable correlation is accessible experimentally.

Idealized models have major advantages for studying correlation effects. First, electron-hole symmetry relates alternating PPP or extended Hubbard models to exact results for regular Hubbard chains, regular or alternating spin-1/2 chains, band theory,

and molecular exciton theory at large alternation. The dimer ( $\delta \sim 1$ ) limit can be readily solved<sup>26</sup> for any U or V(p,p') and differentiates between band-to-correlated crossovers in Hubbard chains, where 1B involves charge transfer between dimers, and PPP or other chains in which 1B is a singlet exciton. The controversial issue of 2A contributions<sup>28</sup> on the correlated side can be studied directly near the dimer limit. Such *theoretical* comparisons near exact limits provide insight and rigorous guidance for extended systems that are unavailable in numerical work.

Second, the large but finite basis of  $\pi$ -electron models allows exact solutions for oligomers, currently to  $N = 14$  sites and electrons.<sup>29</sup> In addition to energies, exact transition dipoles, dynamic NLO coefficients, and other properties are accessible.<sup>30</sup> The quality and range of experimental comparisons using the *a priori* potential V(R) in (2) can be seen for naphthalene,<sup>31</sup> anthracene,<sup>32</sup> *trans*-stilbene,<sup>33</sup> polyenes and their ions, or cyanine dyes.<sup>19</sup> The location of  $2^1A_g$  and other even-parity molecular states relative to  $1^1B_u$  is particularly relevant to the thresholds in Table 1. The location of  $1^3B_u$  and accurate fine structure constants for triplets<sup>31,33</sup> are sensitive quantitative tests of spatial correlations. Oligomer results for other potentials give useful estimates of convergence to the infinite chain and assessments of CI in extended systems. In contrast to approximations developed from band or Hartree-Fock theory, or from correlated localized states, exact solutions span the full range from Hückel to Heisenberg systems, including the spin-charge crossover.

The third advantage of models is their unified approach to polymers. The 2A/1B thresholds in Table 1 follow from Pariser-Parr-Pople theory with constant V(R). The lower energies resulting from greater delocalization in polymers are modeled by treating E(1B) as an internal standard.<sup>34</sup> The ratio E(2A)/E(1B) for 2N-site oligomers decreases or increases, respectively, with N for PPP models<sup>35</sup> with  $\delta < 0.20$  or  $\delta > 0.20$ . The weak N dependence gave the proper 2A/1B ordering of PDA and PPV before direct measurement of 2A in two-photon spectra. As long anticipated from finite polyenes, the lowest singlet excitation of PA is an even-parity state.<sup>36</sup>

To first approximation, correlation effects in conjugated hydrocarbons are comparable for all electrons in  $2p_z$  orbitals. The bond length alternation ( $\delta = 0.07$ ) of polyenes or PA is clearly increased by the  $C\equiv C$  bonds of PDA, whose effective alternation is 0.15. A simple canonical transformation of the Hückel model for PPV shows its large alternation to be topological.<sup>10</sup> A bonding/antibonding pair of MOs is localized on each ring, while an extended alternating chain has transfer integrals  $t\sqrt{2}$  at bridgehead carbons. The Hückel gap of PPV with *equal* bond lengths is larger than the PA gap for  $\delta = 0.07$ . The effects of topological alternation persist in exact Pariser-Parr-Pople states of *trans*-stilbene.<sup>33</sup> The linear absorption of polythiophene suggests that sulfur is a nonconjugated heteroatom. Quantum chemical calculations indicate a charge-density-wave ground state that is reproduced in  $\pi$ -electron theory with a site energy.<sup>37</sup> Since this pushes 2A above 1B in two and three-ring oligomers, as found experimentally,<sup>38</sup> polythiophenes illustrate chemical alternation. An understanding of correlations in alternating chains thus clarifies the energy thresholds of the polymers in

Fig. 2.

## 2.2 Vibronic Structure and NLO Spectra

Conjugated polymers have low excitation energies, large transition dipoles, and strong coupling to C-C stretches. Localized states or excitons are expected to show the diverse vibronic effects found in small molecules. Extended or delocalized excitations, by contrast, have negligible vibronic coupling because many bonds are slightly changed in the excited state. Resolved vibronic structure is consequently evidence for localization. PDA single crystals<sup>20</sup> show resolved sidebands associated with C-C, C=C, C≡C vibrations that also appear<sup>39</sup> in resonance Raman and Raman excitation profiles. Since e-ph coupling is central to the SSH model, vibrational studies have focused on extracting coupling constants and assigning polymer spectra rather than gathering evidence for such coupling. Recent modeling of Raman and infrared spectra of pristine and doped PA indicate quadratic e-ph contributions in  $t''(R_s)$ ,  $t''(R_d)$  for partial single and double bonds.<sup>40</sup>

NLO coefficients are formally given by sum-over-state (SOS) expressions.<sup>41</sup> An  $n$ th-order process contains products of  $n+1$  transition dipoles in the numerator and  $n$  energies in the denominator. The relevant transition moments  $\mu_{sArB} = \langle s^1A_g | \mu | r^1B_u \rangle$  for centrosymmetric chains connect virtual states that are two and one-photon allowed, respectively. The energy denominators have one or three-photon resonances to B states, two-photon resonances to A states. SOS expressions are easily generalized to include vibronic structure.<sup>42</sup> The sums include additional states and transition moments are integrals over both electronic and vibrational coordinates. The Condon approximation reduces transition dipoles to products of electronic moments  $\mu_{AB}$  and Franck-Condon overlaps  $F_{pq}(x)$  between vibrational level  $p$  of A and  $q$  of B in potential wells displaced by  $x$ . The argument holds for any number of normal modes, with vector displacement  $\mathbf{x}$ . The Condon approximation is excellent for dipole-allowed transitions. All potential wells are taken to be harmonic, an approximation that precludes overtone or combination bands. Except in Raman analysis, equal frequencies are assumed in the ground and all excited states. Harmonic oscillators with equal frequencies are convenient<sup>42</sup> because all  $F_{pq}(x)$  are known analytically and practical because few excited-state vibrations are known experimentally. The modeling of vibrational degrees of freedom poses quite different issues that involve all electrons, not just the  $\pi$ -system responsible for large NLO responses.

The analysis of NLO spectra starts with  $\pi$ - $\pi^*$  excitations and transition moments  $\mu_{AB}$  taken from Pariser-Parr-Pople or other models. Oligomers are used in correlated calculations that balance accuracy against size and neglect conformational changes. The idealized alternating chain is now finite. Vibrational inputs come from other measurements when possible. Coupled  $a_g$  modes and  $1B$  displacements are taken from Raman data<sup>39</sup> and resolved sidebands. We have used the three excited states and two coupled modes in Table 2 to fit linear, NLO, and electroabsorption spectra of PDA crystals and films.<sup>43</sup> The same states are suitable for polysilanes<sup>17</sup> and  $\beta$ -carotene.<sup>42</sup>

	State	Energy	Width	Displacement		Dipole with 1B
	$ X\rangle$	$E(X)$ , eV	$\Gamma$ , eV	$x_2$	$x_3$	$\langle X \mu 1B\rangle/\mu_{1BG}$
PTS	1B	2.00	0.025	0.778	0.566	
4BCMU		2.35	0.15	0.95	0.70	
PTS	2A	1.80	0.025	-1.00	-0.75	0.50
4BCMU		1.90	0.15	-1.05	-0.80	0.71
PTS	nA	2.70	0.10	0.8	0.6	1.22
4BCMU		3.22	0.30	0.7	0.5	1.34

Table 2: Excited-state parameters for PDA-PTS crystals and PDA-4BCMU films.

The 1B thresholds in Table 2 are taken from experiment and show a typical blue shift of 0.35 eV on going from crystal to film. The linear absorption of PDA-4BCMU crystals<sup>44</sup> peaks at 1.99 eV and has comparable width  $\Gamma$ . The displacements  $x_2$  and  $x_3$  for C=C and C $\equiv$ C bonds, respectively, are accurately known in crystals and increase in the film. As shown in the top panel of Fig. 3, the stick spectrum based on Table 2 underestimates the 0-1 feature and suggests still larger  $x_2$ ,  $x_3$  in the film. Additional electronic states are expected above 2.6 eV; their inclusion requires more parameters and will be needed at higher resolution.

Resolved two-photon spectra of PDA-PTS single crystals<sup>45</sup> are used to fix the 0-0 excitations for 2A and nA in Table 2. These spectra confirm oligomer calculations<sup>34</sup> showing weak two-photon absorption below 1B and strong absorption around 1.4-1.5 E(1B); the actual value for nA is 1.35 E(1B) and the same ratio holds in 4BCMU films. The transition dipoles in Table 2 are relative to  $\langle G|\mu|1^1B_u\rangle$ , which governs the linear absorption. This suffices for relative NLO intensities, as currently measured. The 2A displacements in Table 2 are guided by two-photon octatetraene spectra.<sup>46</sup> Opposite signs for 2A and 1B displacements improve the fits<sup>43</sup> and suggest an interchange of single and multiple bonds in 2A. The nA displacements and linewidths are quite preliminary.

Excitation energies, transition dipoles, and displacements are sufficient for evaluating any NLO coefficient. Molecular correlation suggests 1B, two even-parity excited states and their transition moments. We then seek a local minimum<sup>43</sup> by adjusting the parameters in Table 2. Transition moments are not quite the same in the crystal and film and thus incorporate interchain or conformational contributions that are beyond an extended oligomer. NLO spectra highlight the tension between detailed fits and a general picture of  $\pi$ - $\pi^*$  excitations, between single-chain models and evident differences in crystals and films, and between electronic and vibrational parameters. In contrast to ubiquitous phenomenological two-level models, the ground and three electronic excitations in Table 2 contain too many parameters to extract a global minimum from the available data. Models with the same number of states may differ,<sup>43</sup> even when fit to the same spectra, because the underlying electronic states are chosen differently.

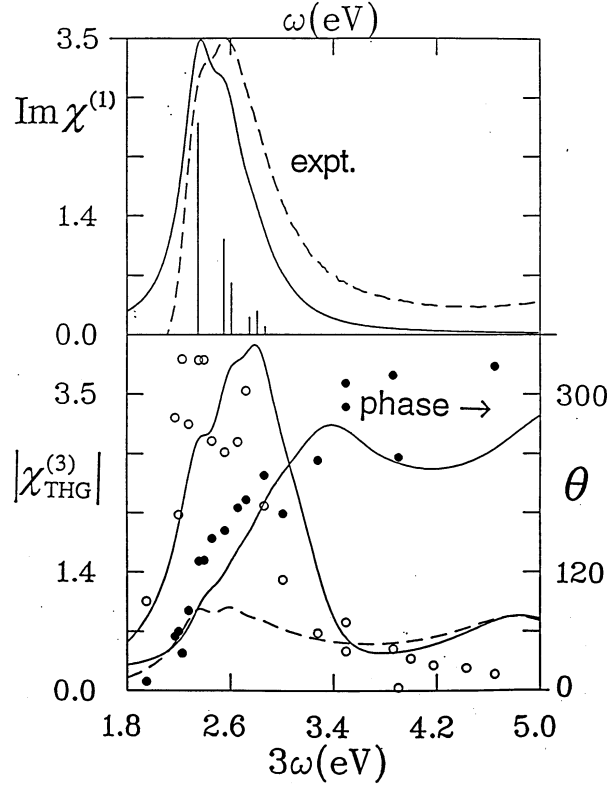


Fig. 3: Top: Linear absorption (dashed line) of PDA-4BCMU films at 300 K and scaled fit (solid line) to 1B in Table 2; the lines are 0-0, 0-1, and 0-2 Franck-Condon factors for C=C and C≡C vibrations. Bottom: THG intensity (open circles) and phase (closed circles) of the same films, from ref. 47. The solid lines are based on the states in Table 2; the dashed line is the THG intensity when 2A is deleted ( $\mu_{2A1B} = 0$ ). (from ref. 43)

The third-harmonic-generation (THG) spectrum<sup>47</sup> of 4BCMU films is shown in the lower panel of Fig. 3. The phase and relative intensity are based on Table 2. The dashed line has the same parameters except for vanishing 2A transition dipoles. Although the calculated moment  $\langle 2^1A_g | \mu | 1^1B_u \rangle$  is small in polyenes,<sup>34</sup> the THG peak around  $3\omega = E(1B)$  in Fig. 3 is enhanced when 2A is below 1B. The two-photon resonance at  $2\omega = E(2A)$  occurs at comparable photon energy and overlaps the three-photon feature. Overlapping resonances require vibronic analysis of simultaneous divergences at  $E(1B) + p\omega_v = 3[E(2A) + q\omega_v]/2$ , for  $p, q = 0, 1, 2, \dots$ . The three-fold THG enhancement in Fig. 3 due to overlapping resonances becomes a six-fold enhancement in  $\beta$ -carotene,<sup>42</sup> where 2A is close to the resonance condition,  $E(2A) \sim 2E(1B)/3$ .

Nondegenerate four-wave-mixing (NDFWM) spectra<sup>47</sup> of PDA-4BCMU films are shown in Fig. 4 at two different frequencies  $\omega_2$  and fit according to Table 2. Since 1B, nA, and 2A are fixed by linear and two-photon spectra, the fits illustrate the

internal consistency of our joint analysis. The major peaks in Fig. 4 are overlapping two and one-photon resonances at  $2\omega_1 = E(nA)$  and  $2\omega_1 - \omega_2 = E(1B)$ . The indicated Raman resonances occur when  $\omega_1 - \omega_2$  matches the C=C or C≡C frequency in Table 2. The Pariser-Parr-Pople analysis of energy thresholds also describes NLO spectra semiquantitatively.

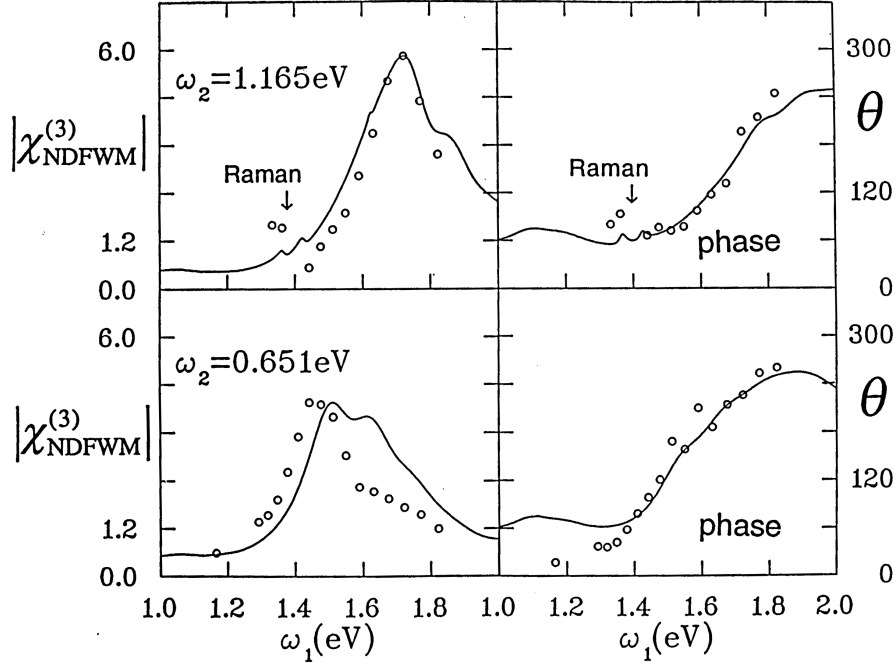


Fig. 4: Amplitude and phase of NDFWM spectra of PDA-4BCMU films, from ref. 47, at  $\omega_2 = 0.651$  and  $1.165$  eV. The solid lines are based on Table 2, with Raman resonances at  $\omega_1 - \omega_2 = 0.20$  or  $0.26$  eV. (from ref. 43)

### 2.3 Stark Profiles of Singlet Excitons

A few resonant states dominate NLO spectra at current resolution. A major exception is electroabsorption (EA), the  $\chi^{(3)}(-\omega; \omega, 0, 0)$  response, whose analysis requires the full spectrum. EA is the change of the linear absorption  $I(\omega)$  in a static electric field  $F$ . Aside from the prominent 1B feature, EA spectra reveal the band gaps of PDA crystals<sup>20</sup> or induced absorption at  $^1A_g$  states of centrosymmetric systems. The Stark shift of 1B leads to familiar  $I(\omega)$  profiles whose analysis gives the polarizability difference,  $\Delta\alpha$ , between  $|1B\rangle$  and the ground state  $|G\rangle$ . The polarizability of singlet excitons in PDA crystals is<sup>20</sup>  $\sim 7000 \text{ \AA}^3$  larger than  $|G\rangle$ , while it is<sup>48</sup>  $\sim 180 \text{ \AA}^3$  larger in poly(di-*n*-hexylsilane). The 1B absorption shifts to lower energy as  $F^2$  in both polymers; the enormous PDA polarizability suggests a highly delocalized e-h pair.

Large transition moments between 1B and higher-energy  $^1A_g$  states are inferred from the red shift. In PDHS, where all even-parity excited states are above 1B, the field-induced lowering of the linear absorption is understood within the PPP

model with Si parameters.<sup>48</sup> These exact results include all virtual  $\pi-\pi^*$  excitations for both 1B and G. The polarizabilities of linear polyenes, where 2A is well below 1B, are also consistent with polymer data.<sup>49</sup> The special feature of PDA crystals is the vibronic overlap of 2A and 1B. The observed PDA-PTS thresholds in Table 1 and  $a_g$  modes in Table 2 account for both one and two-photon absorption at 2.0 eV. Resolved spectra for PDA-PTS single crystals thus demand explicit treatment of vibronic degeneracies.

To model overlapping vibronics in PDA, we retain<sup>50</sup> the states in Table 2 and use the Condon approximation. The perturbation  $V = -\boldsymbol{\mu}\cdot\mathbf{F}$  has matrix elements

$$\langle 2A, s | \boldsymbol{\mu} | 1B, r \rangle = \mu_{2A1B} F_{sr} (b - a) \quad (3)$$

for C=C and C $\equiv$ C overlaps  $F_{sr}$ . The opposite displacements  $b$  and  $a$  inferred from NLO spectra provide a sensitive test. The induced intensity at 1.80 eV, the 2A 0-0 line, is 30 times smaller for opposite signs of  $b$  and  $a$  in (3) than for the same sign. Within the approximation of displaced harmonic oscillators with equal frequencies, it is straightforward to include harmonics for the four electronic states until the EA spectrum converges.<sup>50</sup> More harmonics are needed for 2A and 1B as the total displacement  $|a|+|b|$  increases. As expected from the excitation energies, the vibronic structure of G or nA does not affect the 1B region.

The solid line in the upper panel of Fig. 5 is the EA spectrum,  $I(\omega, F) - I(\omega)$ , based on Table 2 with narrower Lorentzians ( $\Gamma = 0.01$  eV) appropriate at 10 K. The spectrum rigorously scales as  $F^2$  and shows, at three-fold magnification, two 0-1 and three 0-2 sidebands. The dotted line is the calculated first derivative,  $I'(\omega)$ , scaled to coincide with the 2.0 eV EA feature. These theoretical "crystal" spectra deliberately mimic Weiser's experimental data for EA and  $I'(\omega)$  of three PDA single crystals in Figs. 9-11 of ref. 20. The experimental spectra also show coincident EA and  $I'(\omega)$  features for coupled  $a_g$  modes and  $I'(\omega)$  that approximately scales with EA. The Stark shift and  $\sim 7000 \text{ \AA}^3$  change of polarizability comes from the derivative shape and mixing with a *postulated* even-parity state at 2.5 eV, the band gap.

The nA state in Table 2 is above the PDA-PTS band gap and gives an EA contribution that goes like  $I'(\omega)$ . But the crystal simulation<sup>50</sup> in Fig. 5 is dominated by overlapping 2A/1B vibronics whose strong, first-order mixing (3) more than compensates for  $\mu_{2A1B} < \mu_{nA1B}$ . Field-induced absorption at  $|2A, s\rangle$  and bleaching at  $|1B, r\rangle$  are an order of magnitude larger than Stark shifts due to nA. The 1B polarizability is correspondingly smaller. Many implications of correlated states and overlapping vibronics remain to be worked out. The predicted<sup>50</sup> 2A intensity at the location marked in Fig. 5 is close to current experimental sensitivity. The nA feature, by contrast, is masked by overlapping band states starting around 2.5 eV in PDA crystals at 300 K. The strikingly different two-photon intensities of 2A and nA, about 30-fold experimentally<sup>45</sup> and 100-fold in oligomer calculations,<sup>42</sup> is muted in EA because the two processes have different energy denominators.<sup>43</sup>

The lower resolution of films in Figs. 3 and 4 carries over to EA spectra. The upper curves in the lower panel of Fig. 5 are the EA spectrum (solid line) and  $I'(\omega)$  (dotted line) for wider Lorentzians ( $\Gamma = 0.1$  eV) and a 0.35 eV blue shift of all origins, but otherwise identical vibrational levels and transition moments with the crystal curves above. The 500-fold decrease of EA intensity is due entirely to inhomogeneous broadening, which rapidly suppresses derivative features. Sharply reduced EA intensity characterizes polymer films in general; the PDA reduction is consistent<sup>50</sup> with other films.

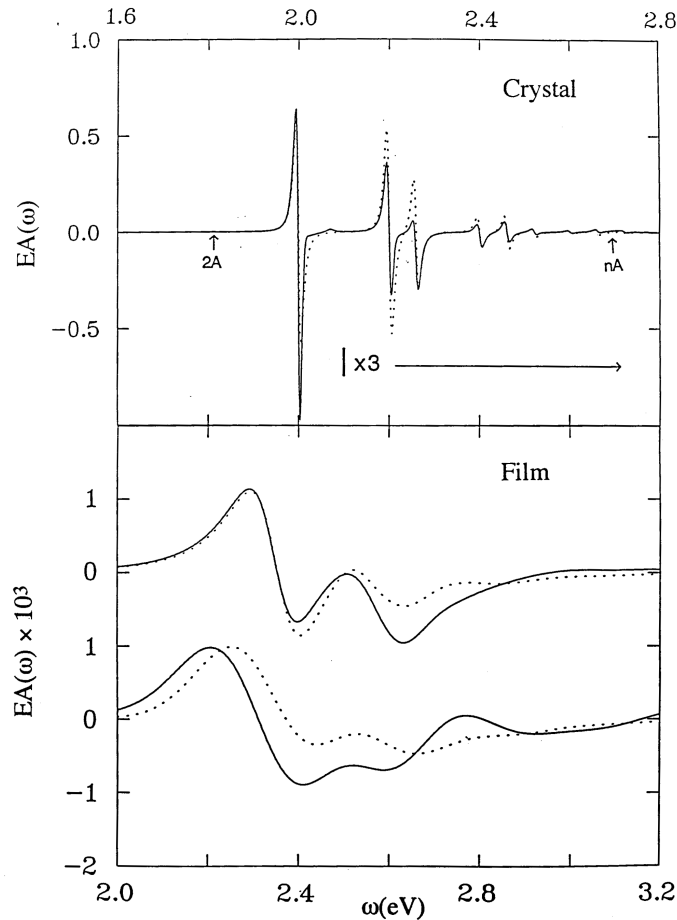


Fig. 5: Top: Electroabsorption spectrum (solid line, arbitrary units) of PDA-PTS crystals using inputs from Table 2 and Lorentzian widths  $\Gamma = 0.01$  eV; scaled derivative (dashed line) of  $I(\omega)$  for the same parameters. Bottom: The upper curves are EA (solid line, same units) spectra and  $I'(\omega)$  (dashed line) for the same inputs except for broader  $\Gamma = 0.1$  eV and a blue shift of 0.35 eV; the lower curves are EA (solid line, same units) and  $I'(\omega)$  (dashed line) for PDA-4BCMU films based on Table 2, as discussed in the text. (from ref. 50.)

The bottom curves in the lower panel of Fig. 5 are based<sup>50</sup> on PDA-4BCMU films from Table 2, with the aim of simulating experimental EA spectra of these

films.<sup>51</sup> The solid line is again the EA spectrum, while the dotted line is  $I'(\omega)$ . The 2A displacements are 30% lower and 0-0 is at 1.86 rather than 1.90 eV. In addition, Lorentzians with  $\Gamma = 0.01$  eV are convolved with a  $\sigma = 0.1$  eV Gaussian obtained from the linear spectrum in Fig. 3. Small changes in the spacing of 2A/1B vibrations alter the 1B feature from a first derivative,  $I'(\omega)$ , to a second derivative,  $I''(\omega)$ ; this transformation is evident because  $I'(\omega) = 0$  is at higher energy than  $EA(\omega) = 0$  in the lower curve. The relative magnitudes of the 2.4 and 2.6 eV dips in the lower EA spectrum agree with experiment on PDA-4BCMU films,<sup>51</sup> which resembles  $I''(\omega)$  at lower energy. A reasonable fit is possible without introducing disorder. The small changes to 2A vibronics to fit the EA do not alter Fig. 4, where 2A contributions are small, but worsen slightly the THG in Fig. 3. Such trade offs and the greater resolution of EA must be addressed for a quantitative fit or understanding.

### 3. EXCITONS IN CONJUGATED POLYMER FILMS

The conjugated polymer spectra in Figs. 3 and 4 are typical of films. There is sufficient resolution to assign spectra, but not definitively. Finite conjugation lengths, segments, and variable environments should be considered; they offer adjustable parameters that produce deceptively accurate fits for a few lines. The EA spectrum in Fig. 5 above 2.8 eV is neither a first nor second derivative of  $I(\omega)$ . This naturally implies contributions from higher-energy states. Until the band gap, disorder or other inputs are independently known, such fits will be difficult to assess. Similar reservations apply to assigning states based on symmetry breaking perturbations without information about coupling strengths. The coincidence of photoconductivity and EA features, for example, gives a more compelling estimate of the band gap than either alone.

The crucial philosophical choice is between quantitative modeling of particular properties or materials, as emphasized in SSH and other solid-state models, and more qualitative fits with transferable parameters, as embodied in Hückel and Pariser-Parr-Pople approaches to conjugated molecules. Ideally, both quantitative and general descriptions follow from quantum cell models. In practice, we have limited fits with generic parameters and more quantitative ones with specific parameters. We must also include disorder or interchain interactions in films without abandoning the advantages of an extended chain or oligomer.

There is circumstantial evidence for excitons in the PPV family. The thresholds of PDA crystals, for example, decisively fix the 0.5 eV binding energy of 1B excitons and their dependence on temperature and sidegroups. The data for PDA films is inconclusive, however, since neither the photoconductivity nor EA has resolved features to mark the band gap. Many of the PPV controversies would also apply to PDA *films*, were it not for the consensus that PDA conjugation is similar in crystals and films. Higher resolution spectra and more inclusive models will clarify the excited states of the PPV family. The similarities of polymers with nondegenerate, centrosymmetric backbones relate PDA crystals to PPV films and suggests singlet excitons. Such reasoning is typical of molecular treatments that we have been extending to conjugated polymers.<sup>10,13,19</sup> The analogy does not provide the 1B binding energy in Fig. 1, nor predict the reversed 1B/2A ordering of PDAs compared to PPVs.

There is other evidence for singlet excitons in polysilanes, as summarized by Kepler and Soos.<sup>52</sup> The band gap of PDHS films in Table 1 is estimated from photoconductivity and EA. Singlet excitons generate carriers in polysilanes, as inferred from the dependence on the photon energy of the photoconductivity quantum yield per absorbed photon. Exciton-exciton collisions generate carriers in PDHS, while exciton-surface generation in poly(methylphenylsilane) resembles the mechanism in anthracene crystals. The appearance of photoconductivity in these films is clearly not associated with the band gap in Fig. 1, which is more than 1 eV higher. The 2A/1B ordering of polysilanes is the same as in PPV, where broad linear absorption and narrow fluorescence also point to excitation transfer to long segments. The side groups in Fig. 2 isolate the  $\sigma$ -conjugated backbone in these polysilanes. The  $\pi$ -conjugated chains in PPV are more exposed and hence prone to interchain interactions or bound polarons<sup>53</sup> on adjacent strands.

### 3.1 Towards quantitative fits and exciton binding energies

General considerations of electronic structure provide a framework for interpreting experiments rather than sharp tests. Quantitative analysis of specific spectra is required to validate any interpretation. Consequently, the appearance of detailed fits of linear and NLO spectra is welcome. A partial list of accurate fits includes NLO spectra for polysilanes<sup>54</sup> using a Wannier exciton model with long-range Coulomb interactions,<sup>55</sup> EA spectra of PPV-MEH using band theory,<sup>56</sup> and NLO spectra of conjugated molecules using orbital methods with CI and vibronic structure.<sup>57</sup> These fits improve the joint analysis in Figs. 3 and 4, especially for the linear absorption  $I(\omega)$ . Coupled-oscillators<sup>58</sup> and essential states,<sup>59</sup> by contrast, focus on general aspects of NLO spectra, without vibronic structure, and are less accurate for PDA-4BCMU films than the fits in Figs. 3 and 4. It is important to consider the number and choice of parameters in comparing current work on conjugated polymers.

Hagler, Pakbaz, and Heeger<sup>56</sup> modeled the linear and polarized EA spectrum of oriented PPV-MEH films. Their  $I(\omega)$  spectrum at 80 K (Fig. 1 of ref. 56) has 1B 0-0 at 2.145 eV, lower than unsubstituted PPV; the vibronics are twice as narrow as PDA-4BCMU films in Fig. 3, but three times broader than in PDA crystals. They emphasize that asymmetric  $I(\omega)$  is inconsistent with the symmetric peak of a  $q = 0$  exciton, the usual selection rule for crystals. Similarly, the spectrum does not show the square-root singularity of band-to-band transitions in one dimension. The asymmetry is quantitatively reproduced by convolution with a symmetric Gaussian. They coupled all band-edge states to a postulated A state at  $E_m = 2.77$  eV to fit the EA spectrum (Fig. 3 of ref. 56), which resembles  $I'(\omega)$  up to 2.4 eV. The resolution is about twice that of the films in Fig.5.

Identical parameters for linear and EA spectra are evidence for long PPV-MEH segments in the oriented sample. The reason is that  $\chi^{(3)}$  coefficients for short segments scale as  $N^b$ , with  $b \sim 4-6$ , and become linear in  $N$  only at large  $N$ , as required by size consistency; but the linear intensity is nearly linear down to small  $N$ . Scaling arguments are independent of transition moments or energies. Such general conclusions

are sometimes possible, even in amorphous materials, by controlling the relative polarizations of photons in two-photon absorption or in polarized absorption and emission. Thus, asymmetric broadening arising from a distribution of segments with slightly different 1B excitation energies is ruled out in the oriented PPV-MEH film.

The obvious question is whether uniform segments also imply a symmetric exciton absorption in flexible strands. The simplest case has  $P$  segments of length  $l$  with transition dipole  $\mu \hat{r}_n$  along the  $n$ th segment for excitation to 1B. Coulomb interactions (2) between charge fluctuations on adjacent segments lead to an exciton band  $-2V\cos q$ , with  $q = 2\pi m/P$ . The molecular crystal limit for parallel segments gives linear intensity  $\mu^2 P$  at  $q = 0$  and vanishing intensity in all other modes. To model flexible chains,<sup>60</sup> we take  $\hat{r}_n \cdot \hat{r}_m = \exp(-\lambda|n - m|)$ , where  $\lambda^{-1}$  is the persistence length in units of  $l$ . The linear intensity for  $N \gg \lambda^{-1}$  is

$$m(q, \lambda)^2 = \frac{\mu^2 \sinh \lambda}{2(\sinh^2 \lambda / 2 + \sin^2 q / 2)}, \quad -\pi < q \leq \pi \quad (4)$$

in the first Brillouin zone. Integration over  $q$  regains  $\mu^2 P$  for  $P$  noninteracting segments for any  $\lambda$ . The maximum intensity at  $q = 0$  is reduced by two at  $q = \lambda$  for small  $\lambda$ , where the absorption energy is  $V\sin^2 \lambda / 2$  higher than the  $q = 0$  exciton.

Flexible strands automatically generate asymmetric exciton profiles in terms of a persistence length  $\lambda$ , an adjustable parameter. Together with the exciton dispersion  $V$ , a good fit of  $I(\omega)$  is expected. Since molecular exciton theory contains first-order perturbations of segment excitations, EA and other responses scale as required with the number of segments. More qualitatively, the observed vibronic structure points to localized states below the mobility edge in a band model, and such edges are difficult to measure. The different thresholds in Table 1 rationalize a coupled A state some 0.5 eV above the 1B exciton. While good fits must follow from successful models, the evaluation of models ultimately rests on their scope. General expressions for two-photon intensities<sup>61</sup> are more complicated than (4) for flexible strands<sup>60</sup> and are required for THG or FWM spectra that depend sensitively on even-parity states. Generalizations of two-level exciton models that include site disorder and multiple excitations have been applied to J-aggregates.<sup>62</sup>

The binding energy, if any, of excitons in the PPV family has been of particular interest,<sup>63</sup> with widely different estimates ranging from  $\sim kT$  to 1 eV. The polaron binding energy  $2E_r$  and exciton binding energy  $E_b$  are referenced to the band gap in Fig. 1 for a free electron-hole pair. The experimental challenge is to obtain accurate results<sup>64</sup> that distinguish clearly among the band gap, polaron pairs, and the exciton. The time scale for charge injection is important. Optical processes are vertical in Fig. 1, while charge injection into polaron states in PA indicates adiabatic states.<sup>65</sup> The interpretation of binding energies raises interesting theoretical questions.

Electrostatic contributions to organic molecular crystals were enumerated in

early studies.<sup>66</sup> The band gap in Fig. 1 is associated with an electron and hole at infinite separation in a solid with the ground-state geometry. It includes a large electronic, or high frequency, polarization energy of  $\sim 0.5\text{-}1.0$  eV per charge in a dielectric medium. Polarization corrections are routinely applied to calculated band gaps<sup>5</sup> or photoelectron levels of oligomers, which lack the surrounding medium. The electronic polarization associated with an exciton is small, since a bound electron-hole is a dipole, and the lattice remains in the ground-state geometry by definition. The electrostatic interaction of the electron and hole is  $e^2/\epsilon R \sim 2$  eV for  $R \sim 20$  Å and dielectric constant  $\epsilon \sim 3$ . The large electronic polarizabilities of separated and nearby charges do not cancel. They are difficult to estimate accurately for states whose delocalization must be found simultaneously.

The coupling constant in polaron theory<sup>7</sup> goes as  $(\epsilon^{-1} - \epsilon_\infty^{-1})$ , the difference between the static and high-frequency dielectric constants, and describes coupling to slow ionic motions. The corresponding contributions to  $E_r$  in conjugated polymers contain both intrachain (molecular) and interchain relaxation. Relaxation also gives a small contribution to  $E_b$ . All-electron calculations are required, as discussed by Suhai<sup>7</sup> for the PDA and PA band gaps. If we imagine the free electron and hole in Fig. 1 to be in different parts of a large crystal, we can relate the band gap to the ionization potential and electron affinity of the polymer; the polarization correction<sup>5</sup> of  $\sim 2.0$  eV then contains major interchain contributions. Even for a single chain, however,  $\pi$ -electron models are not suitable for ionization processes.

In  $\pi$ -electron theory, the  $\sigma$ -core is effectively frozen in the ground state geometry. We model singlet, triplet and other excitations at energies well below  $\sigma$ - $\sigma^*$  processes and work *up* in Fig. 1 from a phenomenological ground state. Delocalization in conjugated polymers improves the separation of active and core electrons by lowering the excitation energies.<sup>19</sup> Such separation for spin degrees of freedom is even better in magnetic insulators and is virtually always assumed for vibrations. The discussion of excited states of neutral conjugated systems also applies to the excitations of their ions, which again allow working up from an electronic ground state. Bond-order changes give qualitative indications of relaxation contributions in  $\pi$ -electron models.<sup>2,33</sup>

In solid-state model models, on the other hand, the band gap is taken from experiment and we work *down* from the gap. The relaxation energy of charged solitons in a Hückel chain with linear e-ph coupling is rigorously given by SSH theory.<sup>22</sup> Relaxation energies of excitons or polarons are typically found numerically for oligomers. Aside from their absolute accuracy, such calculations provide only some contributions to the measured  $E_r$ . The exciton binding energy is modeled by turning on an electron-hole attraction in the Wannier model<sup>55</sup> or a nearest-neighbor  $V$  in extended Hubbard models. Either approach gives parameters for interpreting experimental data that include other effects. The value of simple models is the possibility of obtaining accurate excited states in correlated extended systems. The difficulties of such calculations, even in rigid or harmonic lattices, is illustrated by the different conclusions of recent studies. Yet it is inherently simpler to model  $E_b$  or  $E_r$  than to evaluate either

accurately in actual polymers.

### 3.2 Concluding remarks

We have summarized correlations needed to understand some aspects of linear, NLO and EA spectra of conjugated polymers. Subtle correlations associated with alternating chains yield the 1B/2A ordering that distinguish fluorescent conjugated polymers such as polysilanes or PPVs from the weak or extrinsic emission of PA or PDAs. Long-range Coulomb interactions promote exciton formation in pristine (undoped) polymers and are increasingly replacing Hubbard models for conjugated polymers. The triplet thresholds in Table 1 provide simple tests for exciton or band models. We expect conjugated polymers to resemble organic molecular crystals in this respect, with confined electronic excitations. Exciton motion between segments is related to similar processes in organic molecular solids. The disorder associated with flexible segments and conformational degrees of freedom, on the other hand, resemble traditional nonconjugated polymers. The novel electronic properties of conjugated polymers draw on a unique combination of molecular, band, crystalline, and polymeric features.

Accurate binding energies for excitons or relaxation energies for polarons are interesting current topics, both experimentally and theoretically. As discussed above, they raise basic questions about the adequacy of  $\pi$ -electron models for free electron-hole pairs in conjugated polymers. We anticipate additional studies to clarify the limits of single-strand models, but not to replace  $\pi$ -electron models. As higher resolution spectra become available, additional manifestations of vibronic structure can be expected. Both e-e and e-ph contributions are best understood in simple models that resemble classical Pariser-Parr-Pople theory for conjugated molecules.

### Acknowledgments

It is a pleasure to thank S. Ramasesha, S. Etemad, R.G. Kepler, G.W. Hayden, P.M.C. McWilliams, and D.S. Galvão for many discussions and contributions to correlation studies in conjugated polymers. We gratefully acknowledge support from the National Science Foundation through DMR-9300163.

### REFERENCES

1. R. Pariser and R.G. Parr, *J. Chem. Phys.* **21**, 767 (1953); J.A. Pople *Trans. Faraday Soc.* **42** 1375 (1953).
2. L. Salem, *The Molecular Orbital Theory of Conjugated Systems* (Benjamin, New York, 1966).
3. J. Hubbard, *Proc. Roy. Soc. (London)*, **Ser. A 285**, 542 (1965); **281**, 401 (1964); **277**, 237 (1964); **276**, 238 (1963).
4. Z.G. Soos and D.J. Klein, in *Molecular Association*, Vol. 1, R. Foster, ed. (Academic, New York, 1975) p. 1; D.J. Klein and Z.G. Soos, *Mol. Phys.* **20**, 1013 (1971).
5. J.L. Brédas, in *Handbook of Conductive Polymers*, T.A. Skotheim, ed. (Marcel Dekker, New York, 1986) Vol. 2, p.859; J.L. Brédas, R.R. Chance, R.H. Baughman, and R. Silbey, *J. Chem. Phys.* **76**, 3673 (1982).
6. S. Suhai, *Phys. Rev.* **B29**, 4570 (1984); **B27**, 3506 (1983).
7. C.G. Kuper and G.D. Whitfield, eds. *Excitons and Polarons* (Plenum, New York, 1963); D. Emin, *Advan. Phys.* **24**, 305 (1975).

8. Z.G. Soos, S Ramasesha, and D.S. Galvão, *Phys. Rev. Lett.* **71**, 1609 (1993).
9. B.E. Kohler, C. Spangler, and C. Westerfield, *J. Chem. Phys.* **89**, 5422 (1988).
10. Z.G. Soos, D.S. Galvão, and S. Etemad, *Advanced Mat.* **6**, 280 (1994); Z.G. Soos, S. Etemad, D.S. Galvão, and S. Ramasesha, *Chem. Phys. Lett.* **194**, 341 (1992).
11. A.D. McLachlan, *Mol. Phys.* **2**, 276 (1959); J. Cizek, J. Paldus, and I. Hubac, *Intern. J. Quant. Chem.* **8**, 951 (1974).
12. O.J. Heilmann and E.H. Lieb, *Trans. N.Y. Acad. Sci.* **33**, 116 (1971); S.R. Bondeson and Z.G. Soos, *J. Chem. Phys.* **71**, 3807 (1979).
13. Z.G. Soos, A. Painelli, A. Girlando, and D. Mukhopadhyay, in *Handbook of Conductive Polymers*, 2nd Ed. T.A. Skotheim, R. Elsenbaumer, and J. Reynolds, eds. (Marcel Dekker, New York) in press.
14. R. G. Kepler, in *Treatise on Solid State Chemistry*, Vol. 3, N. B. Hannay, ed. (Plenum, New York, 1976) p. 615.
15. M. Pope and C. E. Swenberg, *Electronic Processes in Organic Crystals*, (Clarendon, Oxford, 1982).
16. R.D. Miller and J. Michl, *Chem. Rev.* **89**, 1359 (1989).
17. R.G. Kepler and Z.G. Soos, in *Relaxation in Polymers*, T. Kobayashi, ed. (World Scientific, Singapore, 1994) p. 100.
18. U. Rauscher, H. Bässler, D.D.C. Bradley, and H. Hennecke, *Phys. Rev.* **B42**, 9830 (1990).
19. Z.G. Soos and G.W. Hayden, in *Electroresponsive Molecular and Polymeric Systems*, T.A. Skotheim, ed. (Marcel Dekker, New York, 1988) p. 197.
20. G. Weiser, *Phys. Rev.* **B45**, 14076 (1992).
21. A.J. Heeger, S. Kivelson, J.R. Schrieffer, and W.P. Su, *Rev. Mod. Phys.* **60**, 781 (1988).
22. W.P. Su, J.R. Schrieffer, and A.J. Heeger, *Phys. Rev. Lett.* **44**, 1698 (1979); *Phys. Rev.* **B22**, 2099 (1980).
23. J.H. Burroughes, D.D.C. Bradley, A.R. Brown, R.N. Marks, K.D. MacKay, R.H. Friend, P.L. Burns, and A.B. Holmes, *Nature* **347**, 539 (1990); D.D.C. Bradley, *Adv. Mat.* **4**, 756 (1992).
24. E.H. Lieb and F.Y. Wu, *Phys. Rev. Lett.* **20**, 1445 (1968).
25. A.A. Ovchinnikov, *Sov. Phys.-JETP* **30**, 1100 (1970).
26. D. Mukhopadhyay, G.W. Hayden, and Z.G. Soos, *Phys. Rev.* **B51**, 9476 (1995).
27. B. Roos and P.N. Skancke, *Acta Chem. Scand.* **21**, 233 (1967); O. Chalvet, J. Hoarau, J. Jousson-Dubien, and J.C. Rayez, *J. Chim. Phys.* **69**, 630 (1972); H. Labhart and G. Wagniere, *Helv. Chim. Acta* **46**, 1314 (1967); K. Schulten, I. Ohmine, and M. Karplus, *J. Chem. Phys.* **64**, 4422 (1976).
28. D. Guo and S. Mazumdar, *J. Chem. Phys.* **97**, 2170 (1992); P.C.M. McWilliams, Z.G. Soos, and G.W. Hayden, *ibid.* **97**, 2172 (1992).
29. Z.G. Soos and S. Ramasesha, in *Valence Bond Theory and Chemical Structure*, D.J. Klein and J. Trinajstić, eds. (Elsevier, Amsterdam, 1990) p. 81.
30. Z.G. Soos and S. Ramasesha, *J. Chem. Phys.* **90**, 1067 (1989).
31. S. Ramasesha and Z.G. Soos, *Chem. Phys.* **91**, 35 (1984).
32. S. Ramasesha, D.S. Galvão, and Z.G. Soos, *J. Phys. Chem.* **97**, 2823 (1993).
33. Z.G. Soos, S. Ramasesha, D.S. Galvão, and S. Etemad, *Phys. Rev.* **B47**, 1742 (1993).
34. S. Etemad and Z.G. Soos, in *Spectroscopy of Advanced Materials*, R.J.H. Clark and R.E. Hester, eds. (Wiley, New York, 1991) p. 87; P.C.M. McWilliams, G.W. Hayden and Z.G. Soos, *Phys. Rev.* **B43**, 9777 (1991).
35. Z.G. Soos, D.S. Galvão, S. Etemad, and R.G. Kepler, in *Electrical Optical, and Magnetic Properties of Organic Solid State Materials*, A.F. Garito, A.K.Y. Jen, C.Y.C. Lee, and L.R. Dalton, eds., *MRS Symposium Proceedings* **328**, 679 (1994).
36. C.A. Halvorson and A.J. Heeger, *Chem. Phys. Lett.* **216**, 488 (1993).
37. Z.G. Soos and D.S. Galvão, *J. Phys. Chem.* **98**, 1029 (1994).

38. D. Birnbaum and B. E. Kohler, *J. Phys. Chem.* **96**, 2492 (1992); **90**, 3506 (1989).
39. D.N. Batchelder and D. Bloor, *J. Phys. C: Solid State Phys.* **15**, 3005 (1982).
40. A. Girlando, A. Painelli, G.W. Hayden, and Z.G. Soos, *Chem. Phys.* **184**, 139 (1994).
41. D.C. Hanna, M.A. Yuratich, and D. Cotter, *Nonlinear Optics of Free Atoms and Molecules* (Wiley, New York, 1984); P.W. Langhoff, S.T. Epstein, and M. Karplus, *Rev. Mod. Phys.* **44**, 602 (1972).
42. Z.G. Soos and D. Mukhopadhyay, *J. Chem. Phys.* **101**, 5515 (1994).
43. D. Mukhopadhyay and Z.G. Soos, *J. Chem. Phys.* **104**, 1600 (1996).
44. M.J. Nowak, G.J. Blanchard, G.L. Baker, S. Etemad, and Z.G. Soos, in *Conjugated Polymeric Materials: Opportunities in Electronics, Optoelectronics, and Molecular Electronics*, J.L. Brédas and R.R. Chance, eds.; NATO ASI Series E **182** (Kluwer, Dordrecht, The Netherlands, 1989) p. 421.
45. B. Lawrence, W.E. Torruellas, M. Cha, M.L. Sundheimer, G.I. Stegeman, J. Meth, S. Etemad, and G.L. Baker, *Phys. Rev. Lett.* **73**, 597 (1994).
46. M.F. Granville, G.R. Holtom, and B.E. Kohler, *J. Chem. Phys.* **72**, 4671 (1980).
47. M. Cha, W.E. Torruellas, G.I. Stegeman, H.X. Wang, A. Takahashi, and S. Mukamel, *Chem. Phys. Lett.* **228**, 73 (1994).
48. R.G. Kepler and Z.G. Soos, *Phys. Rev.* **B43**, 12530 (1991).
49. Z.G. Soos and G.W. Hayden, *Phys. Rev.* **B40**, 3081 (1989).
50. Z.G. Soos, D. Mukhopadhyay, and M.H. Hennessy, *Chem. Phys.* **210**, 249 (1996).
51. A. Horvath, G. Weiser, G.L. Baker, and S. Etemad, *Phys. Rev.* **B51**, 2751 (1995).
52. R.G. Kepler and Z.G. Soos, Chapter 13
53. M. Yan, L.J. Rothberg, F. Papadimitrakopoulos, M.E. Galvin, and T.M. Miller, *Phys. Rev. Lett.* **72**, 1104 (1994); E.M. Conwell and H.A. Mizes, *Phys. Rev.* **B51**, 6953 (1995).
54. T. Hasegawa, Y. Iwasa, H. Sunamura, T. Koda, Y. Tokura, H. Tachibana, M. Matsumoto, and S. Abe, *Phys. Rev. Lett.* **69**, 668 (1992).
55. S. Abe, *J. Phys. Soc. Japan* **58**, 62 (1989); S. Abe, J. Yu, and W.P. Su, *Phys. Rev.* **B45**, 8264 (1992).
56. T. W. Hagler, K. Pakbac, and A.J. Heeger, *Phys. Rev.* **B51**, 14199 (1995).
57. D. Beljonne, J.L. Brédas, M. Cha, W.E. Torruellas, G.I. Stegeman, J.W. Hofstraat, W.H. G. Horsthuis, and G.R. Möhlmann, *J. Chem. Phys.* **103**, 7834 (1995); D. Beljonne, J. Cornil, Z. Shuai, J.L. Brédas, F. Rohlffing, D.D.C. Bradley, V. Ricci, W.E. Torruellas, and G.I. Stegeman, *Phys. Rev.* **B**, (in press).
58. H.S. Wang and S. Mukamel, *J. Chem. Phys.* **97**, 8019 (1992).
59. D. Guo, S. Mazumdar, and S.N. Dixit, *Synth. Met.* **49**, 1 (1992); *Nonlinear Opt.* **6**, 337 (1994).
60. M.H. Hennessy and Z.G. Soos, unpublished results.
61. R.R. Birge and B.M. Pierce, *J. Chem. Phys.* **70**, 165 (1979).
62. T. Tokihiro and E. Hanamura, *Phys. Rev. Lett.* **71**, 1423 (1993); F.C. Spano, *ibid.* **67**, 3423 (1991).
63. C.H. Lee, G. Yu, and A.J. Heeger, *Phys. Rev.* **B47**, 15543 (1993); R. Kersting, U. Lemmer, M. Deussen, H.J. Bakker, R.F. Mahrt, H. Kurz, V.I. Arkhipov, H. Bässler, and E.O. Göbel, *Phys. Rev. Lett.* **73**, 1440 (1994); P. Gomes da Costa and E.M. Conwell, *Phys. Rev.* **B48**, 1993 (1993); M. Chandross, S. Mazumdar, S. Jeglinski, X. Wei, Z.V. Vardeny, E.W. Kwock, and T.M. Miller, *Phys. Rev.* **B50**, 14702 (1994).
64. I.H. Campbell, T.W. Hagler, D.L. Smith, and J.P. Ferraris, *Phys. Rev. Lett.* **76**, 1900 (1996).
65. J.H. Kaufman, J.W. Kaufer, A.J. Heeger, R. Kaner, and A.G. MacDiarmid, *Phys. Rev.* **B26**, 2327 (1982).
66. F. Gutman and L.E. Lyons, *Organic Semiconductors* (Wiley, New York, 1967) Ch.6.